Progress in Solid State Chemistry 49 (2018) 1–15

Contents lists available at ScienceDirect

Progress in Solid State Chemistry

journal homepage: www.elsevier.com/locate/pssc

Molecular structure of Se-rich amorphous films

V.I. Mikla[a], J.M. Turovci[a], V.V. Mikla[a], N. Mehta[b,*]

[a] Humanitarian and Natural Science Department, Uzhgorod National University, Uzhgorod, 88 000, Ukraine
[b] Department of Physics, Institute of Science, Banaras Hindu University, Varanasi, 221005, India

A B S T R A C T

Structure and its transformation are examined for amorphous Se-rich As_xSe_{1-x} ($0 \leq x \leq 0.2$) alloys by employment of diffraction and non-diffraction structural probes. It is shown that the molecular structure of amorphous Se (a-Se) on the scale of short-range order is close to that of crystalline phase, while medium-range order differs from the structure of most inorganic glasses and may be placed between three-dimensional network glasses and polymeric ones. Further experiments show the existence of successive phases in laser-induced glass-crystalline transition with pronounced threshold behavior. Below the energy density threshold, E_{th}, only small changes in the local structure of the system can be detected. Above E_{th}, the changes were attributed to crystallization transformation. The corresponding Raman spectra reveal transformation of the system from amorphous into the crystalline phase under laser irradiation. In the binary As_xSe_{1-x} glass system, a change of structural regime takes place near the composition $x \approx 0.04$. The presence of this topological threshold is established by direct and indirect evidence, such as peculiarities in the composition dependence of the basic parameters for electron diffraction and Raman vibration modes. The peculiarities are caused by the transition from a chain-ring-like structure to preferentially a chain-like structure. Experiments described in this section have shown that Raman technique is a particularly sensitive method to determine the presence of microcrystal's in the glassy matrix. Room-temperature polarized Raman scattering spectra of model glass have been collected. Low-frequency peaks were observed in the spectra. A model is proposed for explanation of their appearance. It is shown clearly that the low-frequency Raman spectra allow determining the conditions at the boundaries, sizes as well as concentration of micro-heterogeneities in non-crystalline materials. It was established earlier that for all amorphous (glassy) materials a low-frequency peak, observed in the corresponding spectral region of Raman scattering and called boson peak, is inherent. This peak is absent in crystals of the same chemical composition and is associated with space correlations on the scale of medium-range order $R_c \approx 10$ Å. On the contrary, less known is that a boson peak can give important information about the presence of microcrystalline inclusions and heterogeneities in the low-frequency Raman spectra of glasses irrespective to their chemical composition.

1. Introduction

Amorphous selenium has been extensively studied over the past 70 years, but its molecular structure is still disputable. For a long time it was believed that the amorphous phase consisted of selenium chain, Se_n, and 8- ring, Se_8, structures mixed together. This model arose from the fact that in the crystalline phase, selenium can exist in two forms, α-monoclinic Se (α-Se) and trigonal Se (γ-Se). The former consisted of Se_8 rings and the latter of Se_nchains. Reasonably, one can consider a structure for the amorphous phase based on a mixture of ring and chain members. However, the length of the selenium chains is uncertain. In addition, it is unclear whether a-Se contains cyclic structure or rings. In recent years there has been enhanced interest in structural studies of chalcogenide glasses owing to their imaging applications. As-containing chalcogenides, especially Se-rich alloys, usually have been studied in thin film form. Since change in the structure can have an influence on photo generation, charge carriers transport, trapping and other important fundamental properties, knowledge of the molecular structure of such materials is needed for further improvement of their characteristics [1–11]. Undoubtedly, elemental semiconductors are useful and suitable testing objects for studying the influence of structure on physical properties [5–7,12–19]. This is particularly true in respect of selenium. In the past, the latter was successfully used in photocells, rectifier diodes and solar cells. In its amorphous form, selenium has a good application as photoreceptor in copying machines and X-ray imaging plates [1,8,11]. Despite the increasing commercial using of a-Se in various applications (see Ref. [8] and references therein), e.g. as promising X-ray flat panel detectors for medical purposes [1], its

* Corresponding author.
E-mail address: dr_neeraj_mehta@yahoo.co.in (N. Mehta).

https://doi.org/10.1016/j.progsolidstchem.2017.10.001

Available online 20 October 2017

structure is not fully understood. On the other hand, binary non-crystalline semiconductors of As-Se system are also of continued scientific and practical interest because of real opportunity of their technological uses (e.g. as functional elements of multi-layer photoreceptors in xerography). Among them the stoichiometric composition, As_2Se_3, and compositions from the range 30–50 at % As are perhaps the most studied ones [12–19]. As for a most of stable binary glasses in As-Se system atomic ratios can be varied in a wide range. Although the information about various physical properties of Se-rich alloys is not so extensive and numerous [5–8,15–20], their compositional dependence manifests extrema or thresholds also in the range 6–12 at % As. It is necessary to accentuate that the As-Se amorphous alloy system display main extrema of various properties at the composition where the valence requirements appear to be satisfied that is at the stoichiometric composition. It seems to be reasonable to connect the mentioned non-monotonic behavior with a specific character of local structure changes. Another prominent feature of the materials studied consists in the following. Certain type of glasses, whose common feature is the presence of chalcogen atoms, sulfur, selenium, and tellurium, exhibit various photo induced phenomena (the reader may refer to K. Shimakawa [10] and Ke. Tanaka [21]). Among these are photo structural transformations and photo crystallization phenomena: a change in optical, electrical and other physical properties is observed. The phase transformation of selenium and its alloys can also be induced relatively simply by laser illumination [22–26]. Reasonably, this unique property makes them attractive for optical data storage and holographic recording. Many experimental results using selenium and its alloys have been reported [27], but few cases of phase transformation properties were mentioned.

In the present chapter electron diffraction and Raman scattering in pure amorphous selenium (a-Se) and Se-rich As-Se amorphous films are reviewed. Below we attempt to clarify the structural transformations induced by light treatment and compositional changes. We focus our attention mainly on photo crystallization transformations. The Chapter also deals with the composition induced structural modifications in amorphous As_xSe_{100-x} or As_xSe_{1-x}. The analysis of electron diffraction and Raman scattering data shows the existence of, some discontinuity of atomic arrangement with rising As content.

2. Techniques exploited in structural studies

Methods used for structural study of solids may be classified into two groups.

2.1. Direct methods

Direct methods include diffraction of X-Rays, electrons and neutrons. The first ones are the methods of determining the arrangement of atoms within a solid, in which a beam of X-rays strikes a crystal and diffracts into many specific directions (Fig. 1).

The incoming beam causes each atom to re-radiate a small portion of its intensity as a spherical wave. If atoms are arranged symmetrically with a separation d, these spherical waves will be only in directions where their path-length difference 2d sin θ equals an integer multiple of the wavelength λ. In that case, part of the incoming beam is deflected by an angle 2θ, producing a reflection spot in the diffraction pattern.

From the angles and intensities of these diffracted beams, a crystallographer can extract information about the mean positions of the atoms in the solid, as well as their chemical bonds, their disorder. Since many materials are solids - such as semiconductors, as well as various inorganic, organic and biological molecules - X-ray crystallography has been fundamental in the development of many scientific fields.

In its first decades of use, this method determined the size of atoms, the lengths and types of chemical bonds, and the atomic scale differences among various materials, especially alloys. X-ray crystallography is still the chief method for characterizing the atomic structure of new materials.

It should be noted here that while diffraction of X-rays, electrons or neutrons gives definite information about the structure of crystalline solids, such measurements give much less information about the structure of amorphous solids [28,29]. The diffraction patterns of amorphous solid consists of diffuse rings whose radial variation of intensity provides a merely one-dimensional representation of the three-dimensional glass structure. Some information about the structure is "averaged out" in the experiments and the structure is surely not 1-to-1 with the diffraction data. In practice one imagines a likely amorphous structure, predicts experiment and compares with the observation. This illustrates the need for the use of many different experimental probes. Diffraction, vibrational spectroscopy and other techniques emphasize different aspects of structure, such as interatomic distance, or angles, or local symmetry, or range of order. Each technique provides an alternative view of the structure and generally averages the structure differently, thus revealing aspects that may be de-emphasized or obscured by another technique. Although each probe gives limited information, the results of several different probes leading to a conviction of truth.

2.2. Indirect methods

Among indirect methods Raman scattering, infrared absorption, extended X-Ray absorption fine spectroscopy and nuclear magnetic resonance can be considered. Raman spectroscopy (named after C. V. Raman) is a spectroscopic technique used to study vibrational, rotational, and other low-frequency modes in a system. It relies on inelastic scattering of monochromatic light, usually from a laser in the visible, near infrared, or near ultraviolet range. The laser light interacts with phonons or other excitations in the system, resulting in the energy of the laser photons being shifted up or down (see Fig. 2).

The shift in energy gives information about the phonon modes in the system. Raman scattering is known to be a powerful technique which give information about local structure of amorphous chalcogenides [30,31].

3. Effect of composition on structure of As_xSe_{1-x} amorphous films: electron diffraction study

In this section, we will discuss the experimental results of electron diffraction and electron microscopic measurements of the structure of As_xSe_{1-x} amorphous films [27,32]. The results of structural investigations of films with low As content have been compared with the literature data.

The samples used in these studies were amorphous films, about 10 μm thick, prepared by vacuum thermal evaporation of the powdered As_xSe_{1-x} melt-quenched material at the rate of 1 μm/min. Freshly cleaved KCl single crystals on the (001) plane were used as substrates. The As_xSe_{1-x} bulk glasses were prepared according to the conventional melt-quenching method with agitating the ampoules content for homogenization. Annealing of the films was carried out in air at ambient pressure and at temperatures 40, 45, 50, 60, and 70° (in Celsius scale) for 0, 2, 5, 10, and 20 at% As, respectively. The composition of the films was determined by electron probe microanalysis, and the composition quoted are accurate to within ± 0.5 at.%. Thin film samples were kept in complete darkness until measured to minimize exposure to light sources, which could lead to changes in the properties and structure of the films. Thermal evaporation method was used due to necessity of reproducing films with chemical composition of glasses. Moreover, the evaporation of As-Se glasses is not of a dissociate character, but it proceeds with fractionation [4]. The temperature T_{ev} of an open-type tantalum evaporator, measured with Pt/Pt-Rh thermocouple, was within $670 \leq T \leq 770$ K depending on glass composition.

The chemical composition of amorphous films was checked by X-Ray spectral microprobe method using the EMMA-4 instrument with a relative error ± 1%. The atomic structure of a film and its changes with

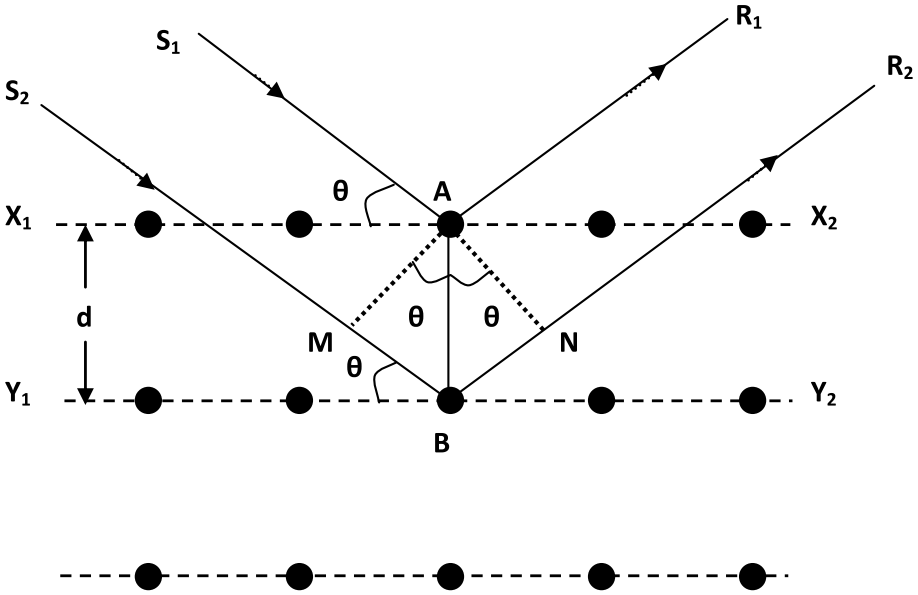

Fig. 1. Illustration of X-Ray diffraction from solids.

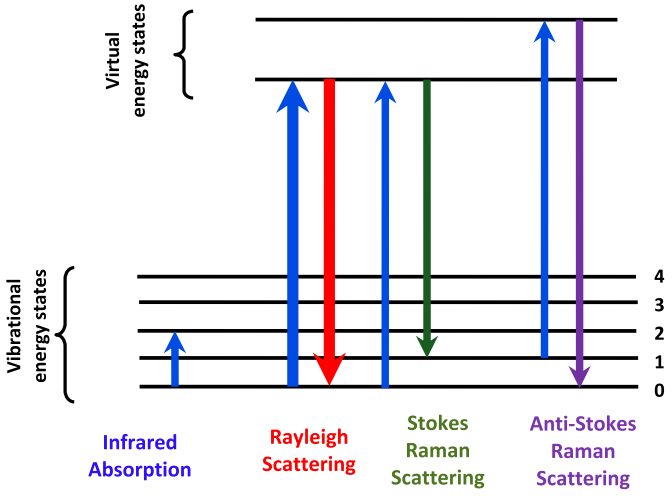

Fig. 2. Visible light scattering from molecules.

thermal annealing were investigated by the electron diffraction method using the EMP-100 instrument and the microstructure was investigated in the EMB-100B transmission electron microscope. It is necessary to note here that the film thickness for structural investigations did not exceed ~600–700 Å.

The short-range order parameters of the atomic film structure were obtained by calculating the radial distribution function (RDF). The dependence I = f (s), where $s = 4\pi \sin\theta/\lambda_e$, θ is the diffraction angle and λ_e is the wavelength of electrons, was plotted in a direct electron current recording mode.

The data about the character and changes in the medium-range order of the atomic film structure were measured by the analysis of positions and intensity of the first sharp diffraction peak (FSDP). The thermal annealing of films was carried out in situ, in the electron diffractometer column.

X-ray spectral microprobe data of the film composition was the same as that of the As_xSe_{1-x} initial glasses (within the measurement error). This similarity showed that quazi-equilibrium evaporation conditions were maintained.

The electron diffraction patterns for As_xSe_{100-x} as-deposited amorphous films at x = 0, 2, 4, 6, 8, 10 and 40 are given in Fig. 3. For comparative analysis we plotted I/I_2 intensity curves, where I_2 is the intensity of the second peak of I (s) curve which is less affected by the natural ageing of films [32].

The data on the analysis of the first sharp diffraction peak position, S_{FSDP}, and the second peak, S_2, and their intensities, I_{FSDP} and I_2, for different compositions of As_xSe_{100-x} amorphous films are given in Fig. 4.

Here circles and square symbols represent the distribution in values of data (for measurements on films prepared with the same evaporation parameters) for compositions with x = 0, 5 and 10. As seen from Fig. 4, the reproducibility of the parameters, S_{FSDP}, S_2, I_{FSDP} and I_2 for different evaporation conditions for films of the same composition is comparatively good.

After thermal annealing of films in situ (in the electron diffraction column), we observed a structural transformation, A1→A2, with retention of the amorphous state, where A1 and A2 were the phase state before and after transformation, respectively. Upon further heating, the films crystallized.

The A1→A2 structural transformation in amorphous chalcogenide films is accompanied by a drastic change in the absorption contrast of the electron microscopic image.

The main difference of diffraction patterns between films in the A2 and in A1 state lies in a complete disappearance of T0 transition for the first sharp diffraction peak, I_{FSDP}, at a certain temperature. In Fig. 3, typical diffraction patterns of $As_{40}Se_{60}$ and As_2Se_{98} amorphous films after A1→A2 structural transformation are shown by dashed lines. New values of S_2 and I_2 for diffraction patterns of As_xSe_{100-x} amorphous films of different compositions after A1→A2 transformation are shown in Fig. 4 by triangular symbols.

It should be noted that diffraction patterns of As_xSe_{100-x} films with low As content after annealing are very similar to those of Se-based bulk glassy samples. This fact is in agreement with the results of Refs. [31,36] in which authors show that the structure of As_xSe_{100-x} deposited films after annealing approaches that of corresponding glasses.

After thermal annealing of As_xSe_{100-x} ($x \leq 10$) amorphous films, the A1→A2 structural transformation occurs even with slight heating caused by electron beam: the films tends to crystallize. It should be noted here that the recording of diffraction patterns for such films in the amorphous state after A1→A2 transformation is difficult.

In Fig. 5 the RDFs of As_xSe_{100-x} amorphous films for $x \leq 10$ are given. The data on the values of the first RDF maximum position, r_1, and area under it, z_1, are presented in Fig. 6. The values of r_1 and z_1 for films with x = 30, 40 and 50 are given for comparison. The corresponding symbols of Fig. 6 are defined in Fig. 4.

The medium-range order of the structure of amorphous films may be characterized to a certain extent by values of S_{FSDP} and I_{FSDP}. From

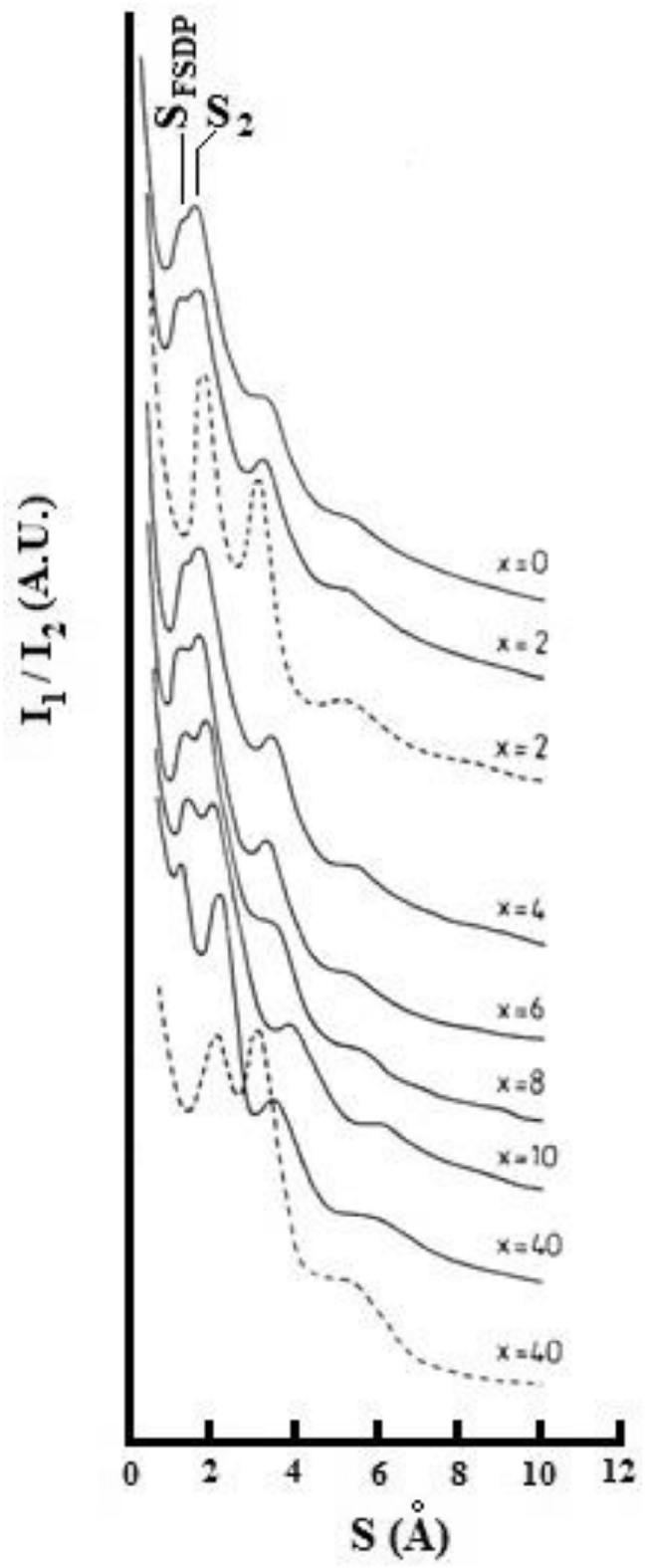

Fig. 3. Electron diffraction patterns of As_xSe_{100-x} as-deposited amorphous thin films (solid line) and films after structural transformation (dashed line) stimulated by thermal annealing. As clearly seen from Fig. 3, the presence of FSDP in the region $S_{FSDP} \approx 1–1.5$ Å is characteristic of diffraction patterns for as-deposited films, and is associated [33–35] with medium-range order of the structure.

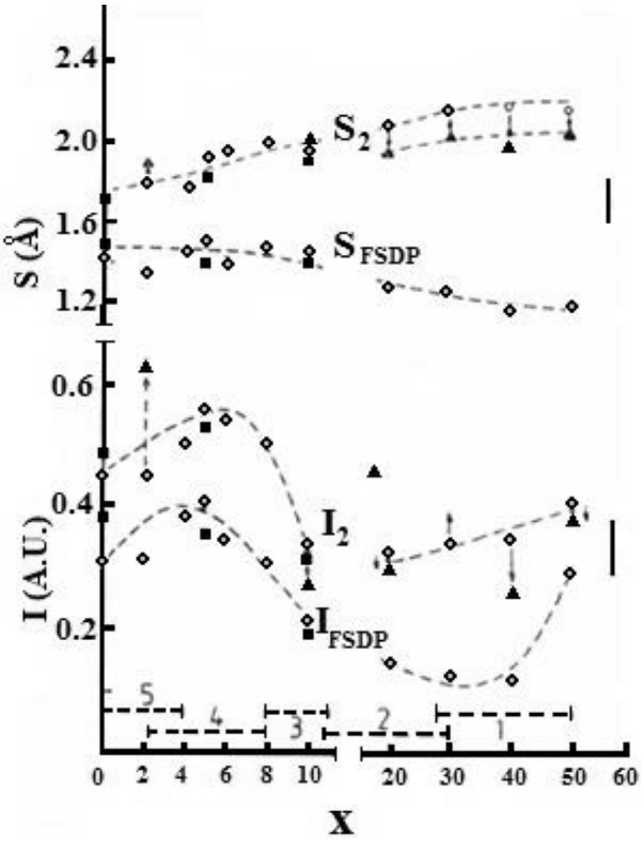

Fig. 4. Dependence of S_{FSDP}, S_2, I_{FSDP} and I_2 on composition for amorphous As_xSe_{100-x} amorphous films. Solid circles and squares are referred to different deposition conditions; solid triangles and open symbols referred to S_2 and I_2 after A1→A2 structural transformation. Lines are guide for eyes.

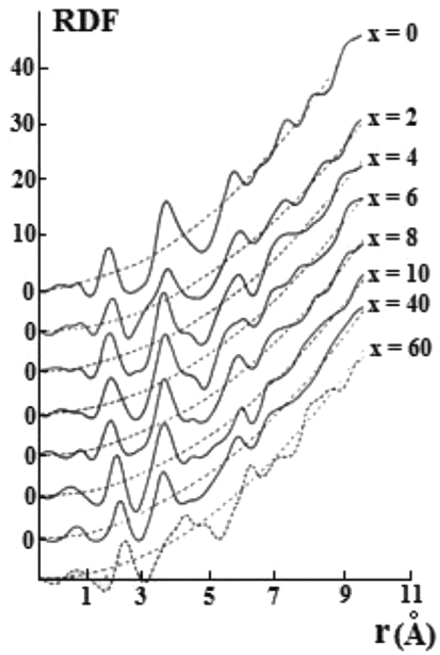

Fig. 5. Radial distribution functions (RDF) of As_xSe_{100-x} as-deposited amorphous films (solid lines) and films after structural transformation (dashed lines) stimulated by thermal annealing.

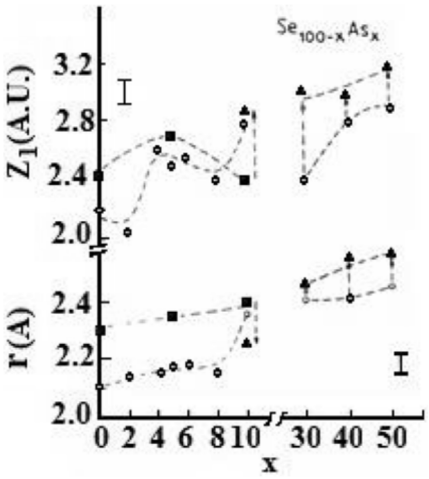

Fig. 6. Compositional dependence of the first RDF maximum position, r_1, and area under it, z_1, for As_xSe_{100-x} amorphous films.

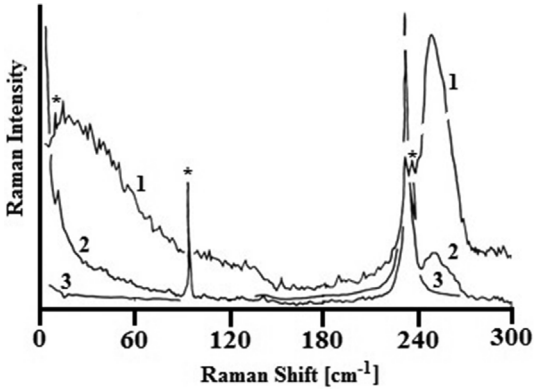

Fig. 7. Here (1) shows the Raman spectra of amorphous selenium, while (2) and (3) are Raman spectra of photo-crystallized selenium. Experimental details for (2) and (3) are: (2) after 5 min exposure of the sample to 10 mW, (3) after 30 min exposure to 10 mW. Asterisks (*) indicate laser plasma lines.

the analysis of Fig. 4, it follows that As_xSe_{100-x} as-deposited films in the composition range $0 \le x \le 10$ and $20 \le x \le 50$ differ in a correlation length, $L = 2\pi/S_{FSDP}$, of the medium-range order and in the degree of medium-range ordering.

The FSDPs for amorphous films of composition close to $As_{40}Se_{60}$ are explained in the approximation of the cluster model. According to this model the correlation length, L, is associated with the size of quasi-molecular (cluster) species in the structure of as-deposited films [37].

In the region of low As content, the calculated values of correlation length are $0.42 \le L \le 0.46$ nm, whereas for the region of compositions $30 \le x \le 50$ one obtain $0.50 \le L \le 0.55$ nm. The latter is fairly well fitted [38] with the distance between the "furthest" Se atoms in As_nSe_m quasi-molecular species ($n = 4$, $m = 6$). The average value of L in the composition range $0 \le x \le 10$ correlates with the sizes of Se_6 molecules and with the average distance between Se_nchains in the structure of amorphous selenium [4].

We suppose that the peculiarities observed in composition dependence of structural characteristics for As_xSe_{100-x} films with low As content are conditioned by a topological structure of the disordered network to appear in those local regions where linking, branching of chains and formation of closed rings occur. Generally, this results in an increase in the intensity of the main diffraction peak I_2 and peak IFSDP. The latter is assumed to be responsible for the medium-range order, and in a mutual change in the position of these peaks.

4. Raman scattering in pure and alloyed amorphous selenium: case study of high-frequency spectral region

Raman scattering is a very powerful experimental technique for providing information on the constituent structural units in a given material [30]. In the present section the Raman scattering in pure amorphous selenium (a-Se) and Se-rich As-Se amorphous films are studied. Below we attempt to clarify the structural transformations induced by light treatment and compositional changes. We focus our attention mainly on photo crystallization transformations. In addition, the composition-induced structural modifications in amorphous As_xSe_{1-x} are also analyzed. As shows the detailed analysis of Raman data, some discontinuity of atomic arrangement with rising As content exists.

The samples used in these studies were amorphous films, about 10 μm thick, prepared by vacuum thermal evaporation of the powdered As_xSe_{1-x} melt-quenched material at the deposition rate of 1 μm/min onto quartz substrates held at room temperature as well as polished mirror-like parallelepipeds of vitreous As_xSe_{1-x}. The As_xSe_{1-x} bulk glasses were prepared according to the conventional melt-quenching method. Annealing of the films was carried out in air at ambient pressure and at temperatures below the glass-transition temperature. Thin film samples were kept in complete darkness until measured to minimize exposure to light sources, which could lead to changes in the properties and structure of the films. It is important accentuate that after annealing procedure their Raman spectra become indistinguishable from the corresponding spectra of melt-quenched glassy samples. It should be noted that for Se-rich compositions studied only slight difference in the spectra of melt-quenched and as-deposited samples is observed.

Right-angle Raman spectra were measured using RAMANOR U-1000 spectrometer. The spectral slit width was ~1 cm^{-1} and the excitation wavelength 676 nm. Laser beam of sufficiently low incident power P = 3–5 mW is focused into 100 μm spot. In other words, Raman spectra of the amorphous films were recorded with sufficiently low incident laser-beam intensity $I = 1.3 \times 102$ W/cm^2 to avoid photo structural changes. The latter is known to transform the Raman spectra. The identity of the experimental spectra obtained from different points of the sample and the good reproducibility of the spectra in repeated scans (the time required to scanning one spectrum in the spectral range 100–300 cm^{-1} is about 5 min) show that photo darkening did not play a role in the subsequent Raman measurements.

The structure of photo-crystallized films was investigated using X-ray diffraction.

In Fig. 7, a typical Raman spectrum of a-Se measured at low incident radiation power density, ~3 mW, is shown. The stable level of the scattered light intensity and the good reproducibility of the spectrum in the repetitive cycles clearly indicate the absence of any structural changes in a-Se induced by laser irradiation of such power density. On the high-frequency side (ω = 100 to 300 cm^{-1}) the spectrum contains an intensive peak at 255 cm^{-1} and some peculiarity (shoulder) at 237 cm^{-1}.

The above features are in good agreement with previously reported data [39–43]. In the low-frequency region one can observe the broad peak with ω_{max} = 16 to 20 cm^{-1}. This so-called boson peak occurs in the low-frequency region of the Raman spectra of all amorphous and vitreous solids. We considered this spectral region in separate paragraph.

When we try to identify certain vibration bands observed in the Raman spectrum of a-Se, some difficulties arise. Initially it was proposed to interpret the a-Se Raman spectrum by analogy with sulfur – on the basis of a molecular approach (see Fig. 8). That is, the main vibration band was considered to be the superposition of the peaks at 237 and 255 cm^{-1} characteristic of chains and rings, respectively [41]. However, further experimental data have caused some doubts to be cast. In such a case one would expect to observe a discernible difference in the contributions of 237 and 255 cm^{-1} mode to the main vibration

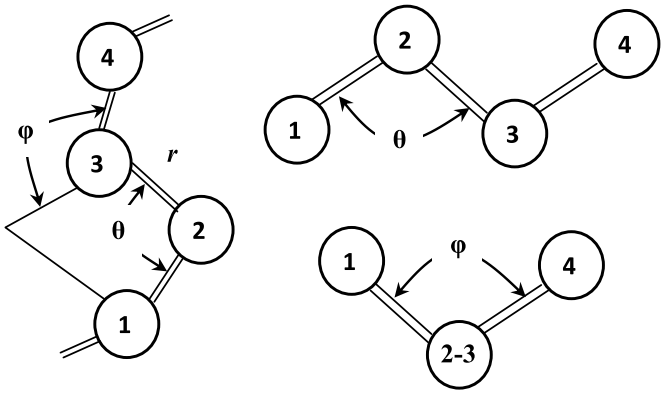

Fig. 8. Se chain molecule and definition of the dihedral angle ψ. The definition involves an angle between planes and thus four atoms labeled 1, 2, 3 and 4. It is observed looking down the bond joining atoms 2 and 3.

band in the samples prepared at different conditions (e.g. substrate temperature during deposition for amorphous films or quenching rate for glassy samples). This may be caused by changes in rings to chains ratio. Therefore, it is clear that the spectral region 200 to 300 cm^{-1} is unsuitable for ring diagnostics. This is consistent with the conclusions of [42].

The Se_8 peak (112 cm^{-1}) could not be detected in the present experiment. Probably, this is connected with its weakness. This fact indicates evidently the low concentration of rings. Consequently, one can associate the spectral features in the main vibration band, the 255 cm^{-1} peak and the shoulder at 237 cm^{-1}, mainly with the chain vibrations (see Fig. 9).

In the present section experimental results on Raman scattering spectra for Se-rich amorphous semiconductors As_xSe_{1-x} are also discussed. In Fig. 10 typical Raman spectra of amorphous Se and As-Se alloys with As content up to 5 at % are shown. The major spectral feature in the high-frequency region is the 255 cm^{-1} band. Another prominent spectral feature which is not shown in this Figure is the

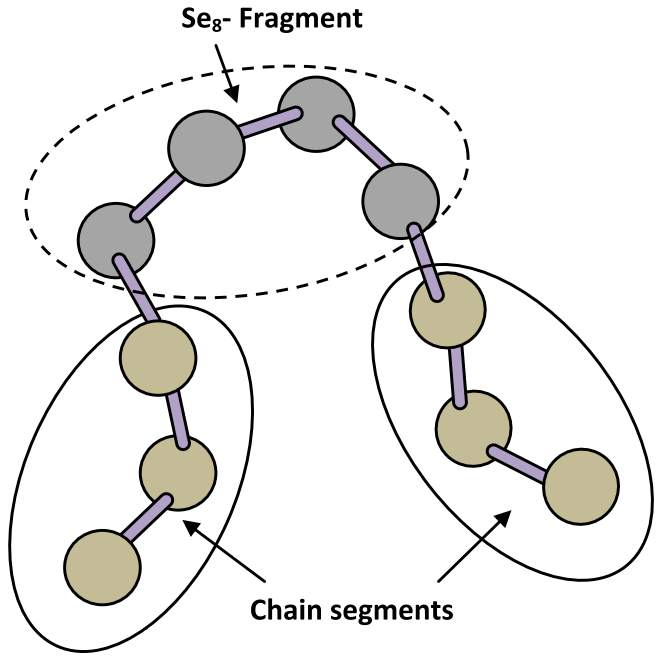

Fig. 9. Local molecular order in a selenium chain in which there are segments characterized by repetition of the same dihedral angle ("chain-like" in the sense of trigonal Se) and segments characterized by alternating dihedral angle ("ring-like" in the sense of Se_8 molecule).

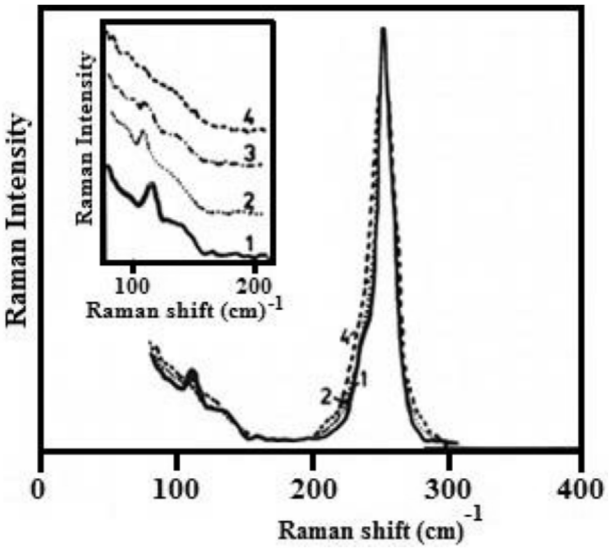

Fig. 10. Comparison of the Raman spectra of (1) amorphous Se and As_xSe_{1-x}: (2) x = 0.02, (3) 0.04, and (4) 0.05 at %. Each trace has been normalized to the same peak (255 cm^{-1}) intensity. The inset shows the bending mode region.

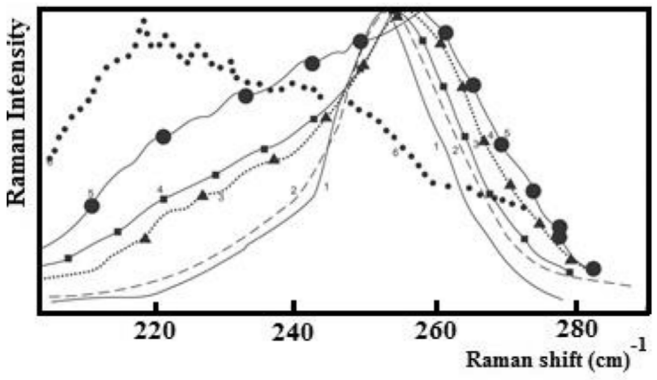

Fig. 11. Raman spectra of amorphous As_xSe_{1-x} films annealed at $T = T_g$. (1) x = 0 (solid line), (2) 0.05 (dashed line), (3) 0.10 (dashed-doted line), (4) 0.12 (dashed double-doted), (5) 0.20 (solid circles), and (6) 0.40 (points). We have used these unconventional denotations for Raman spectra to be distinguishable.

broad peak at ω_{max} = 16-20 cm^{-1}. As mentioned, the latter is characteristic for Raman scattering of all amorphous solids and glasses.

In the following we consider only the high-frequency region. The weak feature observed at 112 cm^{-1} in the a-Se spectrum diminishes with As addition and at 5 at % completely disappears (see inset Fig. 10). At the same time the difference in the spectra in the region of the main vibration band is obvious. Thus, with increase of As content the transformation of the Raman spectrum in this region is retraced (Fig. 11).

The most important points are as follows:

i. Spectrum broadening with increasing As addition.
ii. Growth of scattered light intensity from the low-frequency side of the main maximum (255 cm^{-1}).
iii. Appearance of a broadened band at 220-230 cm^{-1} (this band is the most intense in the Raman spectrum of $As_{0.4}Se_{0.6}$). It should be noted also that the main maximum is slightly shifted to higher frequency for amorphous As_xSe_{1-x} respectively to Se (255 cm^{-1}).

The intensity of the 220-230 cm^{-1} band in the As concentration interval 0–5 at % remains practically unchanged. Then, at 6 at % As, an increase of the band intensity occurs. A gradual intensity rise is

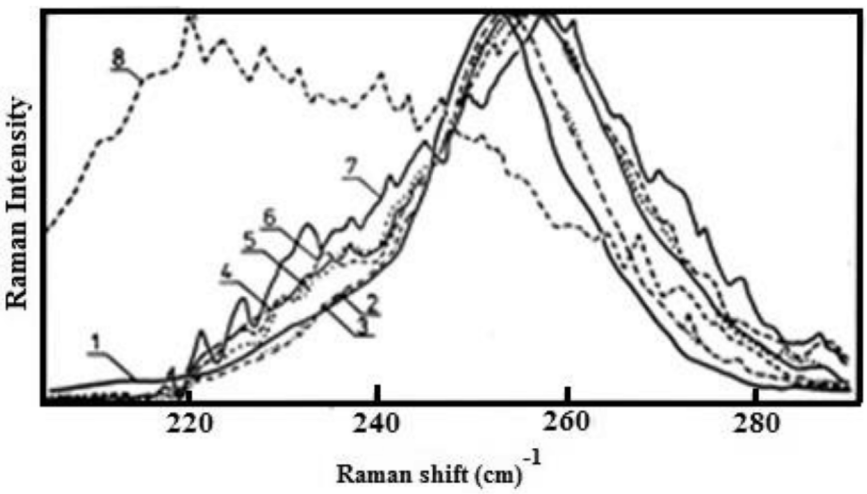

Fig. 12. The difference spectra (for details see the text) for a-As_xSe_{1-x}. x = 4, 5, 6, 8, 10, and 20 at %, curves 2 to 7, respectively. For the sake of comparison Raman spectra (1) a-Se and (8) $As_{40}Se_{60}$ are also shown.

observed for the band at 220 cm^{-1} as the As content is further increased. For As content exceeding 35 at % the band dominates in the Raman spectrum.

The corresponding calculations have been performed (the scattered intensity was determined as $I(As_xSe_{1-x}) = I(Se) + K \times I(As_{0.4}Se_{0.6})$, where the normalization coefficient K was appropriately estimated or each composition) for amorphous materials under investigation. These calculations yield that a systematic discrepancy between approximated and experimental spectra is observed. As for the latter, the greater values of the main peak width are typical.

Fig. 12 shows difference spectra obtained by subtracting the $As_{0.4}Se_{0.6}$ spectrum from experimental Raman spectra. The relative contribution of the $As_{0.4}Se_{0.6}$ spectrum was fitted to the ~230 cm^{-1} region where the contribution from pure Se was negligibly small. It is obvious that after such a procedure some peak remains, width and position of which differs from that for a-Se.

Based on the data given in Fig. 12, values of the parameter A were estimated. This parameter represents the ratio of the integrated Raman intensity in the interval limited by the typical frequencies $AsSe_{3/2}$ unit vibrations (205 and 230 cm^{-1}) to the integrated intensity of the whole spectrum of valence vibrations:

$$A = \frac{\int_{205cm^{-1}}^{230cm^{-1}} di}{\int_{205cm^{-1}}^{290cm^{-1}} di}$$

Note that this is done after normalizing each spectrum.

Fig. 13 shows that the dependence A ~ f(x) is non-monotonous –parameter A increases around ~ 6 at % As. For the frequency range 240–270 cm^{-1}, the change of scattered intensity with composition has a smoother character. On the same figure, the dependence of the peak frequency, ω_{max}, and its width, $\Delta\omega_{max}$, on As content for the corresponding spectra is displayed. It is important to note the similarity of the composition dependence of A, ω_{max}, and $\Delta\omega_{max}$.

An attempt to simulate As_xSe_{1-x} Raman spectra by a superposition of two constant spectral forms one of which belongs to a-Se, the other to $As_{0.4}Se_{0.6}$ failed. Onari et al. [44,45] was first who used a similar approach. On the contrary, the experimental spectra could be approximated assuming a considerable broadening of chain vibrations and their frequency displacements. We consider that such an approach is correct and that the difference spectra themselves are convincing arguments in favor of it: the change of the Raman spectra with composition together with parameters A, ω_{max}, and $\Delta\omega_{max}$ (see the corresponding figures) support this suggestion.

Composition-dependent studies on the physical properties of binary and ternary chalcogenide glasses give evidence for the existence of mechanical and chemical thresholds at certain compositions of these

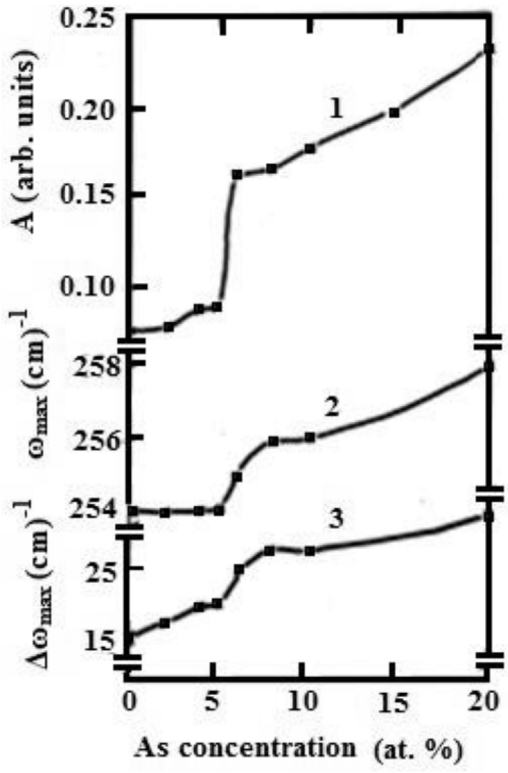

Fig. 13. Compositional dependence of the parameters A (1), ω_{max} (2), and$\Delta\omega_{max}$ (3). (1) On the basis of experimental data, (2), (3) from calculated curves of difference spectra.

materials [46–48]. The As-Se system displays main extrema of various properties at the stoichiometric composition (the mechanical and chemical thresholds coincides at x = 0.40).

There seem to exist (see experimental results published by Kasap [49] and present data) an additional threshold at 0.06 ≤ x ≤ 0.12. It can be argued that the non-monotonic behavior observed in the concentration dependence of glass transition temperature, density, etc. [50] in this range originates from changes in bond topology [46,49]. We assume that in Se-rich glasses the network is dominated by Se atom chains (quasi-one-dimensional network) and addition of As atoms lead to branching owing to threefold coordination of As atoms. Recent publications [49,51,52], as we believe, give a new approach to the problem of local bonding in amorphous chalcogenides. The anomalous behavior near x ≈ 0.06 is ascribed to the disappearance of Se_8-like segments. From the point of view of configuration, it is suggested that

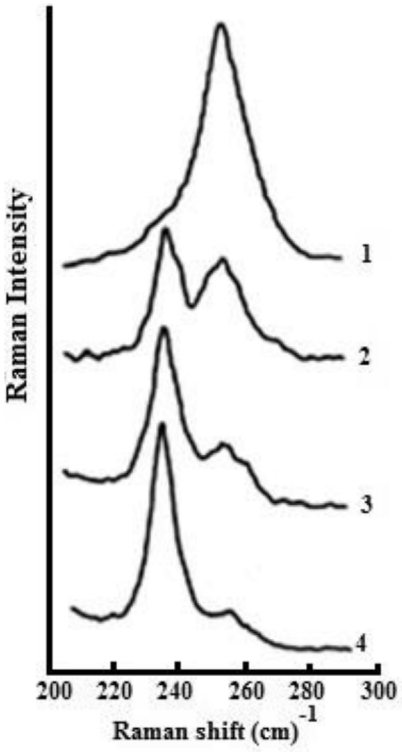

Fig. 14. Laser-induced transformation of Raman spectra of amorphous Se. Experimental details for (1)–(4) are: (1) reference spectrum of amorphous state, (2)–(4) after exposure to E = 3.8, 11,4 and 19 × 10^3 J/cm^2, respectively. I = 1.3 × 10^2 W/cm^2.

the number of cis-configurations in rings starts to decrease, so that the mediate-range correlation is modified. The considerable reduction in the vibration mode at ~112 cm^{-1} associated with cis-segments in ring component strongly supports this suggestion.

Changes in the Raman spectrum with composition allow us to conclude that incorporation of As leads to cross-links between chain-like or ring-like segments of amorphous Se.

There are strong indications that the compositional dependence of physical and chemical properties has no connection with chemical ordering. In fact, the binary As_xSe_{1-x} alloys exhibit extrema in compositional dependence of the density not only at the $As_{0.4}Se_{0.6}$ composition, but also for the non-stoichiometric chalcogen-rich $As_{0.06}Se_{0.94}$ and also for pnictogen-rich $As_{0.6}Se_{0.4}$ samples. This means that the x dependence of the density originates from changes in bonding topology.

We may summarize the general features of the observed transformation of Raman spectra in the range of bond bands for amorphous selenium. 1) There is (as shown in Fig. 14) certain threshold energy, E_{th}, of the incident radiation. 2) Below E_{th}, no changes of Raman spectrum are observed. Here we note that the only exception is the so-called boson peak detected at around 17 cm^{-1} which is weakened by illumination. 3) Above E_{th}, an increase of the incident energy density modifies the spectra.

The present experimental results permit to distinguish three successive stages of photo-crystallization in a-Se with regard to irradiation energy density. First of all it is necessary to point out the absence of any significant structural transformations in films and bulk samples at E_{th} ≤4 J/cm^2. This is strongly supported by the identity of the Raman spectra recorded in repetitive cycles. At the first stage, which is induced by irradiation with incident energy density ≥3.8 J/cm^2, micro crystallite formation probably takes place. In such a case the 255 cm^{-1}peak dominates the Raman spectra. The second stage of photo crystallization (~11 J/cm^2) is characterized by an enlargement of microcrystalline units. This is demonstrated by the growth of the 237 cm^{-1} peak. Finally, at ~20 J/cm^2, photo crystallization practically takes place. This stage is marked by a dramatic increase and narrowing of the peak at 237 cm^{-1} with irradiation time. At the same time, the 255 cm^{-1} peak becomes more and more suppressed with respect to other.

Raman active modes and, finally, it completely disappears. At this last stage of photo crystallization the absence of the low frequency (17 cm^{-1}) peak is also characteristic.

It seems to be reasonable to assume a thermal, caused by laser heating of the sample, mechanism for the observed structural transformation. This suggestion is strongly confirmed by the clearly manifested threshold behavior. Additional support comes from the fact that at low temperature the threshold power (e.g. 20 J/cm^2 at T = 100 K for a-Se) which is necessary for changes in Raman spectra to be observed exceeds several times that for changes at T = 300 K. Note that the changes under examination qualitatively differ from the well-known photo darkening phenomena. As for the latter, it takes place at any value of irradiation power; threshold behavior was not characteristic of them. The magnitude of photo darkening depends mainly on the amount of absorbed energy and significantly increases with temperature lowering. The relatively greater efficiency in films in comparison with bulk samples is established feature of photo darkening. In contrast, in our case, the threshold power densities for a-Se films are found to be higher than for bulk samples. According to results [53,54], discernible reversible photo darkening in a-Se at T = 100 K occurs at photon energy hν ≥2.0 eV with maximum efficiency at ~2.4 eV. Probably, the exciting irradiation energy, hν = 1.84 eV seems to be low to induce significant photo darkening at T = 100 K. At the same time the probability of transient photo darkening effects relaxing after finishing the irradiation at T = 300 K for E ≈ 3.8 J/cm^2 cannot be definitively ruled out.

With regard to As_xSe_{1-x} Raman data, principal results are as follows

i. The spectra of the As_xSe_{1-x} amorphous alloy samples before irradiation were the same as those reported in Refs. [15,31,40,42–45].
ii. The value of E_{th} necessary for changes in Raman spectra to be observed vary with addition of As (see Table 1 given below).
iii. Under irradiation with E > E_{th} the recorded spectra clearly show a narrowing and increase in the intensity of the 237 cm^{-1} Raman band.
iv. In As_xSe_{1-x} samples with x ≤ 0.05, no additional (to that recorded for pure Se) photo induced changes in their Raman spectra are observed (see Fig. 15 and compare with the results for a-Se). It should be accentuated that, on introducing such a relatively large quantity of As additives, there is no appreciable influence on the photo crystallization product. It is well known that Se is likely to be photo crystallized at ~350 K [22,50]. Reasonably, X-ray diffraction patterns of the samples have been measured. Since the illumination region is of ~3 mm in radius, the pattern is noisy. However, we can clearly see four crystalline peaks located at 2θ = 24°, 30°, 41°, and 45°. The peaks can be indexed, respectively, as 100, 101, 110, and 111 of the trigonal (hexagonal) Se crystal [55].
v. For As content > 15 at%, the main result of this study is the appearance and disappearance of new Raman bands typical for $As_{0.4}Se_{0.6}$.

Table 1
E_{th} values as a function of As concentration in As_xSe_{1-x} alloys.

As concentration (at.%)	E_{th}[a] (kJ/cm^2)
0	2 ± 1
5	12 ± 3
8	7 ± 2
12	8 ± 2
20	45 ± 5

[a] The E_{th} values are shown for the case I = 1.3 × 10^2 kJ/cm^2.

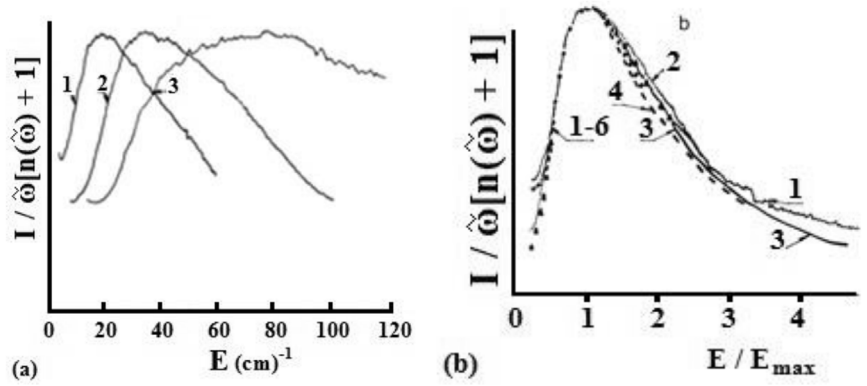

Fig. 15. Development of the photo crystallization effect in $As_{0.05}Se_{0.95}$ as a function of exposure: 1, reference spectrum of amorphous state; 2, 3, after exposure to 15, 20 and 25 × 10^3 J/cm^2, respectively. I = 1.3 × 10^2 W/cm^2.

For example, Fig. 15 shows the appearance of an additional peak (~264 cm^{-1}) superimposed on the amorphous peak (~255 cm^{-1}). With a further increase of the irradiation energy density, crystallization starts immediately. Here we should note an evolution qualitatively similar to that shown for pure Se and $As_{0.05}Se_{0.95}$ in the shape of spectra over the concentration range 0–20 at %. In the final stage of photo crystallization, the spectra of As_xSe_{1-x} alloys are free of key crystalline features that occur [56] in the spectra of crystalline As_2Se_3. It is of particular significance that only the 237 cm^{-1} band of trigonal selenium contributes to the spectra of photo crystallized As_xSe_{1-x} ($0 < x < 0.20$) films.

We define E_{th} (e.g. E_{th} = 2 × 10^3 J/cm^2 at I = 1.3 × 10^2 W/cm^2 in the case of pure Se) as the energy density for which the system is not yet perturbed structurally (on the scale of short-range order) by laser irradiation. The absence of any significant bonding changes in films is supported by the identity of the Raman spectra recorded in repetitive cycles. This result holds for both pure amorphous selenium and Se-rich As_xSe_{1-x} alloys. For energies less than E_{th} reversible photo darkening and transient transmission changes are observed. These effects are characteristic of the amorphous phase and the system remains in the amorphous phase under or even after irradiation. The lack of any noticeable variation in the transient behavior T_{rel} for samples of different substrate material and film thickness exclude the possibility of the effect being due to small changes in sample temperature during and after illumination, i.e., to photo induced heating.

We have recently reported similar dynamical photo induced changes in some photo electronic properties detected by time-of-flight and xerographic technique [18–20,57]. These experiments may provide the first evidence that deep defects can be altered temporarily by room-temperature irradiation. Note that there is a close correlation between the recovery of optical parameters and photo electronic characteristics in exposed samples.

Although a complete correlation of microscopic structural modifications with macroscopic photo darkening phenomena must await further experimental measurements, it is only natural that we relate the transient changes in the transmissivity with changes in deep defect states. We identify such centers as arising from native (thermodynamic) structural defects (e.g., C_3^+ and C_1^- in amorphous selenium). Band-gap light can probably initiate conversion of traps of small cross-section to those of larger cross-section [8,58].

By contrast, above E_{th}, all the observed irreversible changes may be attributed to optical constant variations and modifications in the kinetics of light-induced crystallization.

The present experimental results resolve successive stages of photo crystallization in a-Se (these were mentioned above). In such a photo crystallization process, amorphous Se undergoes a transformation to the trigonal selenium which is the most stable modification. Raman scattering studies together with X-ray diffraction data gave an unambiguous indication of trigonal selenium.

On the basis of the present Raman data, we conclude that the features of the photo crystallization effects in As_xSe_{1-x} alloys with $x < 0.15$ are qualitatively the same as those in amorphous selenium. Some deviation in pre-crystallization behavior of $As_{0.2}Se_{0.8}$, namely the appearance and disappearance of the weak quasi-crystalline peak at 264 cm^{-1}, probably indicates As_2Se_3-like cluster creation and annihilation. The latter could be clusters with a more ordered structure with respect to that existing in amorphous phase. At the same time, they are not yet micro crystallites with inherent Raman peaks. It seems to be reasonable that the environment of the clusters prevents their growth and transformation into micro crystallites. Other Se clusters reach the critical size required for micro crystallite formation. After that, sample exposure to $E > E_{th}$ crystallized selenium, while the As-containing clusters remained in amorphous phase. The above explanation is in agreement with the results of the study of laser-induced structural transformations in glassy As_2Se_3 [58] and also with the mechanism proposed by Phillips [59].

It is known [50] that As is an effective additive to decrease the tendency to crystallization. Our experimental results, namely the greater value of E_{th} for a-As_xSe_{1-x} films, indicate that the addition of As effects the suppression of the crystal nucleation and growth in amorphous selenium. The long Se chains in amorphous selenium branch at the site of As atoms. The length of Se chains becomes short [45,60] and the amorphous Se cannot easily crystallize with increase of As concentration.

At the same time, it is necessary to note that the changes in optical transmissivity and diffraction efficiency that occur are not monotonic with increasing As content. It seems to be reasonable to connect such a behavior with some discontinuity of atomic arrangement with increasing As content. Our recent study of composition dependence of Raman bands in amorphous As_xSe_{1-x} supports this suggestion.

5. Raman scattering in pure and alloyed amorphous selenium: case study of low-frequency spectral region

It has become evident that traditional techniques of structural investigation are inefficient for study of disordered materials. They give information on the structure of a short-range order only and are slightly sensitive to more long-range correlations in arrangement of atoms. The existence of the medium-range order is admitted: periodical atomic arrangement inherent in crystals remains within several coordination spheres and then is violated. It is assumed that the character of the violation may depend on preparation and chemical composition of the sample [28,61]. A number of experimental procedures were proposed, for measurement of a size ordered micro regions, or structural correlation range R_c. One of these methods permits to determine R_c by the position of a low-frequency boson peak in Raman spectra [62]. It has been shown [61–63] that the Raman intensity can be described by

$$I/\varpi(n(\varpi)+1) = \sum_b C_b(\varpi)g_b(\varpi)/\varpi^2$$

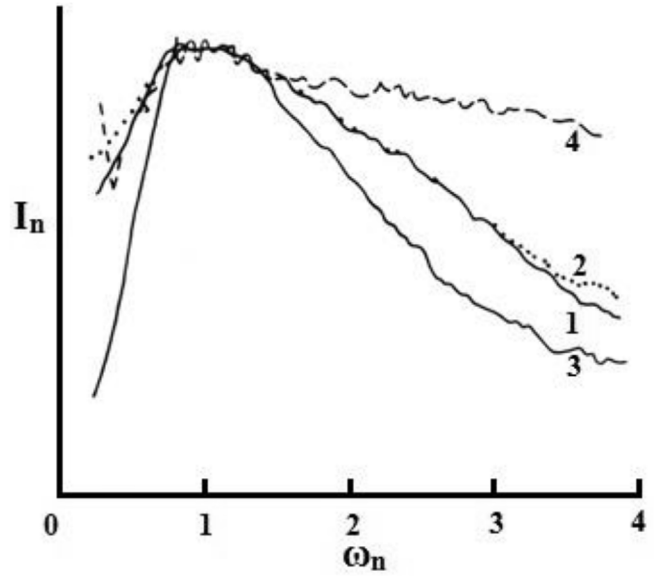

Fig. 16. (a) Low-frequency Raman spectra of As_2S_3 – 1, $Bi_4Si_3O_{12}$ – 2, $La_2S_3Ga_2S_3$ – 3 glasses [61]; (b) Raman spectra of different glasses in a scale $E_n = E/E_{max}$: 1 – As_2S_3 (E_{max} = 26 cm^{-1}), 2 – $Bi_4Si_3O_{12}$ (34 cm^{-1}), 3 – SiO_2 (52 cm^{-1}). In addition it is shown spectrum: 4 – B_2O_3 (28 cm^{-1}), 5 – B_2O_3 (45 cm^{-1}), 6 – GeS_2 (22 $cm^{-1)}$ and 7 – Li_2O (88 cm^{-1}) [61].

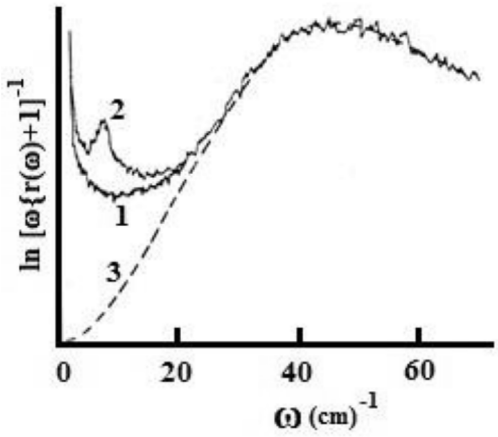

Fig. 17. Low-frequency Raman spectra of different glasses in a scale $\varpi_n = \varpi/\varpi_{max}$. (1) Se ($\varpi_{max}$ = 17 cm^{-1} at T = 100 K), (2) Se (ϖ_{max} = 17 cm^{-1} at T = 300 K), (3) As_2S_3 (ϖ_{max} = 26 cm^{-1}, T = 300 K), (4) polymethylmetacrylate (PMMA) (ϖ_{max} = 17 cm^{-1}).

Here g_b is the density of states and C_b is the matrix element of the coupling of the vibration mode b to the light, $n(\varpi)$ is the boson occupation number. In the low-frequency region $I/\varpi(n(\varpi)+1) \sim \varpi^2$ increases and then reaches a maximum at certain value $E = E_{max}$ (Fig. 16a), which depends on chemical composition and thermal prehistory of the sample [63,64]. This peak was called in literature as a boson peak. It accounts for 30–90% of integrated intensity of Raman spectrum in glasses.

Authors [61] have compared spectral form of the low-frequency band in various samples. For the sake of simplicity all the spectra are given in the same energy scale $E_n = E/E_{max}$ (Fig. 16 (b)). A unique property of the boson peak was found: in a broad frequency range the spectral form of the peak is independent of chemical composition of the sample. Additional analysis of results (Fig. 16 (b)) indicates that the boson peak has a universal nature, which is due to the most general features of vitreous structure and is not associated with the concrete chemical composition of glass or with the structure of corresponding crystal. One of these features is the medium-range order. Universal form of the boson peak is assumed to be due to this general character of vitreous solids.

The low frequency region $0 < \omega < 100$ cm^{-1}, in which the boson peak appears in a-Se, is of special interest. It has been found that the spectral form of the boson peak is nearly the same for a wide series of oxides, chalcogenides, and low-weight molecular organic glasses. The universal form of the low frequency peak is due to universality of glassy material in the scale of medium-range order $L \sim \upsilon/\varpi_{max}$ = 1–2 nm (υ is the sound velocity). For the case of a-Se, it is observed (Fig. 17) that the spectral form of the boson peak essentially differs from that characteristic of the majority of inorganic glasses. The spectral form of the boson peak in a-Se seems to be intermediate between that in polymeric and low-molecular glasses.

Normalized Raman spectra $I_n = I/\varpi(n(\varpi)+1)$ for a-Se and series of other composition samples are given in the same energy scale $\varpi_n = \varpi/\varpi_{max}$, where $n(\varpi)+1 = [\exp(h\varpi/kT)-1)+1]^{-1}$ is the boson factor for the Stokes component.

This result can be explained by a preferentially chain-like structure of a-Se. The latter may form a structure similar to the structure of linear polymers PMMA. In other words, with regard to its structure on the scale of medium-range order, a-Se may be placed between 3-dimensional network glasses and polymeric ones. Examples of mediate-range order in elemental and compound materials, including a-Se, have been extensively discussed in Refs. [65–70].

There exists another possible explanation. Selenium has its glass transition temperature near room temperature; therefore it is in a well annealed state. It is known [61] that the intensity of the boson peak relative to the main bond modes in the Raman spectrum significantly decreases as the structural order of the sample increases (e.g. in "equilibrated" or annealed samples). This decrease in turn may lead, respectively, to an increased contribution from other modes to the high-frequency side $\varpi > \varpi_{max}$ of the boson peak. This is clearly seen if we compare the shape of corresponding peaks in a-Se and As_2S_3 (Fig. 17).

6. Finite size microcrystals in glasses

Relatively great number of studies has been performed to understand the structure of non-crystalline solids from light scattering investigations. The majority have concentrated on spectral features in the optical mode region of the Raman scattering spectra. Recent interest has developed in the low-frequency or acoustic Raman modes region. This interest is a manifestation of theoretical works on the properties of light scattering from acoustic modes in disordered solids [71,72]. A direct explanation for the universal presence of low-frequency modes in non-crystalline modes was given by Shuker and Gammon [1] and Martin and Brenig [72] (the later authors exemplified it for the case of oxide glasses). Studies appeared on other aspects of Raman scattering as a sensitive probe for the structure of glasses. To the author's best knowledge, Duval [73] was the first who established that Raman spectroscopy is a powerful and sensitive technique to determine the size of the microcrystal's in a glass. It has been shown that, in the case of microcrystals included in a glassy phase, only the lowest energy vibration eigenmodes (surface modes) are active in the acoustic Raman scattering region [74–76]. Interestingly, the frequency of these surface vibration modes (modes with large amplitudes at the particle surface) are related to the diameter of the microcrystals.

The low-frequency Raman spectra of glasses with microcrystals have been investigated in this paragraph. It is shown that the spectra permit to determine conditions at the boundaries, sizes and concentrations of structural microinhomogeneities in disordered materials.

Model glasses ($K_2O{\cdot}Al_2O_3{\cdot}6GeO_2$, Photochromic glasses, chalcogenide glasses) were chosen as samples for these studies for several reasons. These materials can be prepared as well characterized high optical quality bulk glasses. Optical quality is important to minimize the spectral component due to elastically scattered light which masks low frequency Raman spectral features. In addition, both glasses can be

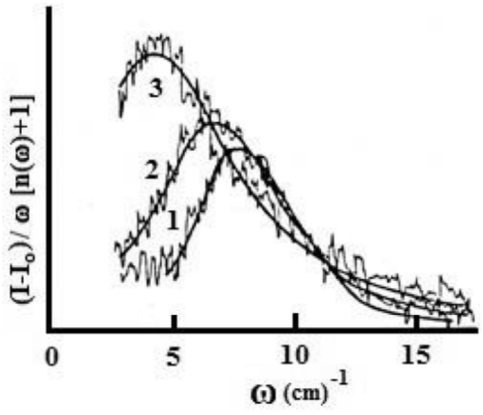

Fig. 18. The low-frequency Raman spectra of the not-annealed (1) and annealed (2) samples; (3) – the calculated spectrum [77] for the contribution from acoustic vibrational excitation.

easily prepared and crystallized. Fortuitously, one can study properties aroused from differences in structure (caused by thermal treatment) in detail.

Right angle Raman spectra were performed in the usual VV and HV polarizations.

Fig. 18 shows Raman spectra for the not-annealed and annealed photochromic glass samples. A low-frequency (the so-called boson peak, typical of the spectra of any vitreous material) is observed at the frequency $\omega \approx 60\ \mathrm{cm}^{-1}$.

Annealing of samples caused a change of the spectra in the frequency range $\omega < 20\ \mathrm{cm}^{-1}$; the peak with $\omega_{\max} \sim 10\ \mathrm{cm}^{-1}$appears. The latter corresponds to vibrational spectrum of microcrystals which grow during annealing (see Fig. 19).

Clearly, the amplitude of the low-frequency peak increases while decreases with annealing temperature.

In general, the annealed samples contain inhomogeneities of two types. The first corresponds to inhomogeneities of matrix itself. The second is associated with microcrystals (See Fig. 20).

The results obtained can be interpreted in terms of phenomenological model. Let us consider homogeneous medium. The density-of-states, $g(\omega)$, is described by the Debye's law

$$g_0(\omega) = 3\omega^2 2\upsilon^3\pi^2, \tag{1}$$

Here $\upsilon=(\upsilon_t^{-1}2/3 + \upsilon_l^{-1}/3)^{-1}$, with υ_t and υ_l being transverse and

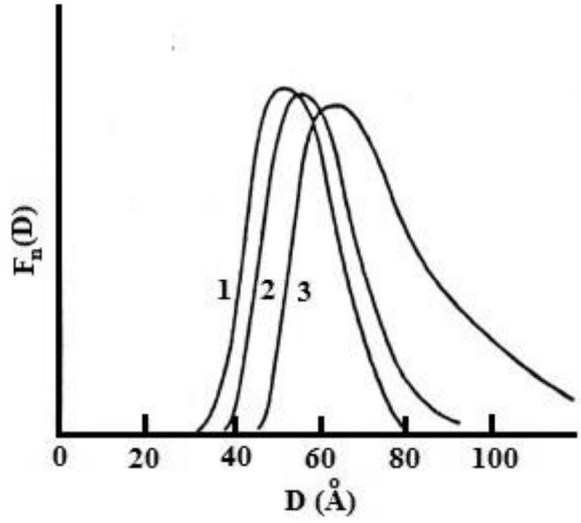

Fig. 19. The difference between spectrum of not-annealed sample and spectra of samples: annealed during 2 h at: 550° C (1), 573° C (2) and 600° C (3).

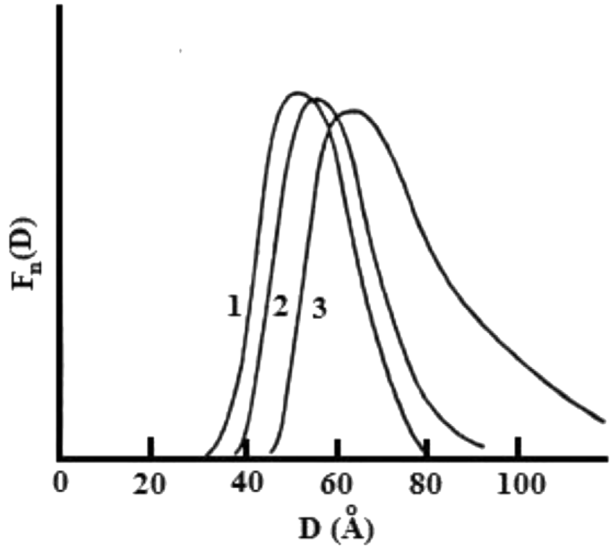

Fig. 20. Distribution functions of microcrystal's size in the samples. Numeration of the curves is the same as in Fig. 19.

longitude sound velocities, respectively. The presence of microcrystals in glassy matrix changes the Debye density-of-states. There appear additional low-frequency modes due to surface vibrations of microcrystals. These modes are localized at $\omega \approx \upsilon/D$. To describe their contribution to the density-of-states, a simple phenomenological model is used.

The form of the microcrystals is assumed to be close to spherical ones of D_0 in diameter. The density of vibrational states, with account of the contribution from low-frequency modes of a sphere vibrations ω, can be written in the form:

$$g(\omega) = g_0(\omega) + N\delta(\omega - \omega_0). \tag{2}$$

Both the finite lifetime and the scatter in sizes and shapes of microcrystals results in the broadening of vibrational modes. We can express the Lorentz distribution of width Γ in the form:

$$g(\omega) = 3\omega^2/2\upsilon^3\pi^2 + N\Gamma((\omega - \omega_0)^2 + \Gamma^2)^{-1}/\pi. \tag{3}$$

As evident from Eq. (3), there is the resonant peak at$\omega = \omega_0$, superimposed on the smooth Debay density of states.

In disordered materials, the Raman intensity is proportional to the density of vibrational states $g(\omega)$ [71]

$$I_0(\omega) \sim C_{ij}(\omega) g(\omega)(n(\omega) + 1)/\omega, \tag{4}$$

HereC_{ij} is the square of matrix element of light interaction with vibrational excitation, $n(\omega) + 1$ is the bose-factor.

In the low-frequency range, for the acoustic vibrations

$$C(\omega) \sim \omega^2, \tag{5}$$

And the factor of proportionality depends on elasto-optic constants P_{ij} of the material [78]. Assuming Eq. (5) for simplicity, we have

$$I/\omega(n(\omega) + 1) \sim g(\omega). \tag{6}$$

The frequency of a spherical mode, $I = 0$, is related to the sphere diameterD_0 as follows:

$$\omega_0 \cong 0.7\upsilon_c/cD_0, \tag{7}$$

Here c is the light velocity. Spherical and torsional modes have the frequency:

$$\omega^l = \omega^t \cong 0.85\upsilon_t/cD_0. \tag{8}$$

Therefore, the Raman intensity is of the form:

$$I(\omega_0)/\omega_0(n(\omega_0) + 1) \approx (P_{ij}^g)^2 3\omega_0^2/2\upsilon^3\pi^2 + P_{ij}^m N/\pi\Gamma. \tag{9}$$

Here P_{ij}^{g} and P_{ij}^{m} are elasto-optic constants of the glass and micro-crystal, respectively. In Eq. (9), the first term corresponds to the scattering on acoustic phonons of the glass I^{ac}, while the second is the contribution of vibrations localized on micro-crystals I^{loc}. Therefore, one can estimate: a) microcrystal sizes using the position of the localized mode in Raman spectrum ω_0; b) the microcrystal concentration for Γ and I^{loc}/I^{ac} given:

$$N \cong (I^{loc}/I^{ac})(P_{ij}^{g}/P_{ij}^{m})^2 3\omega_0^2\Gamma/2\upsilon^3\pi. \quad (10)$$

The model predicts the lowest surface modes to be localized at $\omega_{max} = \beta/D_0$, where $\beta \approx 10^{-6}$.

It seemed that the appearance of spherical or torsional modes is determined by interaction between the microcrystal surface and the surrounding glassy matrix: spherical modes if the glass matrix is softer than the microcrystal; torsional for the case of weak coupling between the microcrystal surface and the environment.

In addition to D_0, the Raman spectrum allows to estimate the microcrystal concentration for I^{loc}/I^{ac} given. It is well-known [79] that a central peak make considerable contribution to the intensity of light scattered at room temperature in the range $\omega < 20$ cm^{-1}. Contribution from acoustic vibrations can be separated via approximation of the boson peak. Taking all factors into account, one obtains $N \approx 10^{17}$ cm^{-3}.

Finally, the low-frequency Raman scattering appears to be a sensitive method for the investigation of the initial stage of nucleation in multi- and mono-component systems [79]. In the case of the mono-component systems, when the crystalline nuclei do not have an acoustic mismatch as compared to the amorphous matrix, we cannot observe their surface vibrations, but we can make use of the fact that in nucleation there is a jump in a structure correlation length. This results in a sharp decrease in contribution to the density of the acoustic vibration states because of decreasing the concentration of structural correlations on which acoustic phonons are localized. In addition, low-frequency Raman spectroscopy may be useful in the research into the phase transformation in materials for phase-change memories. From the fact that the 17 cm^{-1} band is the only observed in a-Se, does not contain microcrystalline-related features which shift in frequency or increase in intensity with thermal treatment, it may be deduced that all our Raman spectra correspond to the advanced stages of crystallization. That means Raman spectra do not show the formation of the very small microcrystal's or nuclei but only reflect the more advanced crystal growth process.

7. On the origin of boson peak

The boson peak is a broad peak found in the low-frequency region of Raman scattering spectra in a wide range of many solid state materials, including amorphous films, inorganic glasses, liquids/melts, polymers/bio-polymers, and partially crystalline materials [80–87]. The peak is recognized as a universal feature of very different amorphous materials. Here, we give a state of the art of the low-frequency (Boson) peak.

Light scattering can be used to obtain information about the static structure and the dynamics of gases, crystals, liquids, amorphous solids, glasses and polymers.

It is well-known that all glasses and polymers and even some disordered crystals exhibit excess vibrations in the terahertz frequency range. The density of vibrational states at these frequencies far exceeds the expectation of the Debye model. The latter is based on a simple assumption of homogeneous isotropic elastic continuum. Despite the long history of studies, the microscopic nature of these low-frequency vibrations remains a subject of active discussions [88–102]. In fact, these discussions started already some 50 years ago with the observation of a low-frequency Raman band that usually is not present in crystalline Raman spectra and which has been called “boson peak”.

Among general features inherent to disordered solids the so-called Boson peak (BP) is the most intriguing. It is observed in the inelastic photon (Raman & X-ray) and neutron scattering spectrum in a THz frequency range and is recognized as a universal feature of quite different amorphous materials such as, e.g., glasses, polymers, supercooled liquids or even amorphous ice.

Another important topic that is ultimately connected to the nature of the excess vibrations is the attenuation of the sound-like waves at the frequencies of the boson peak In particular, the connection between the damping of the vibrational modes, the plateau in the low temperature thermal conductivity, and the boson peak itself, is still highly debated. A new interest to these topics has been inspired by recent developments in experimental techniques and theoretical approaches. Also, the observed correlations between the terahertz dynamics and the peculiarities of the glass transition fragility call for additional attention to the microscopic mechanisms controlling the fast dynamics.

Vitreous materials like silica, boric oxide and soda-lime-silica glass are the classic materials from which both the physics of the amorphous state and the modern concepts of atomic structure of glass originated.

In an amorphous solid, Shuker and Gammon [86] showed that the first order Raman scattered Stokes intensity could be written as

$$I(\omega) \approx [C(\omega)g(\omega)/\omega](n(\omega) + 1)$$

where $C(\omega)$ is the coupling coefficient, $g(\omega)$ is the density of states and $n(\omega)$ is the Bose-Einstein thermal population factor.

The Boson peak can be defined as an excess contribution to the usual Debye density of states (DOS). The name is give because the temperature dependence of the intensity of the peak follows that of a harmonic oscillator characterized by the Bose factor. It can be observed with a variety of optical, neutron and thermal measurements, including Raman spectroscopy.

Krishnan observed in 1953 the boson peak with Raman scattering [94]. He found for v-SiO_2 a broad band in the vicinity of 30–120 cm^{-1} (note that 1 THz = 33.35 cm^{-1}) which markedly differs from the behavior of crystals.

Because the Raman light scattering is an electronically driven process, not all the vibrations will be able to interact with the incoming light. The intensity of Raman scattered light depends not only on the vibrational density of states, but also on the coupling between photons and vibrations.

Disordered solids, especially glasses, are compelling materials to study from a fundamental point of view as they pose challenging and yet unsolved problems in the field of condensed matter physics. Ranging from silicates to halides and chalcogenides, inorganic glasses have found amazingly widespread use in our lives that ranges from windshields, flat-panel displays and electric bulbs all the way to optical fibers and amplifiers in modern day telecommunication networks. Vitreous materials like silica, boric oxide and soda-lime-silica glass are the classic materials from which both the physics of the amorphous state and the modern concepts of atomic structure of glass originated. From a historical standpoint silicate glasses are the most ancient materials known to mankind. They also occur naturally, predominantly amongst volcanic rocks, and indeed offer important insight into the physic-chemical conditions in the interior of our planet. At the other extreme, chalcogenide and halide glasses represent some of the most recent functional materials to be discovered.

In the last decades our understanding of the static atomic structure of amorphous solids has advanced substantially. These advancements have been due primarily to huge improvements in experimental methods like Raman spectroscopy and elastic and inelastic neutron scattering.

All of these experimental advances reveal a wealth of order, both at the local level of individual structural entity as well as in the intermediate range governed by the connectivity's between adjacent units. The discovery of sources of more distant or longer-range order in inorganic glass systems is an additional exciting development.

Fundamental physical properties of amorphous solids differ strongly

from those of crystals. An interesting feature of their vibrational dynamics is a broad band observed in Raman scattering spectra in the low-frequency region. This band is identified as the boson peak. The origin of this boson peak, as mentioned above, is still under debate.

Vibrational properties of disordered materials are one of the currently lively topics of modern condensed matter physics. Features of the disordered vibrational spectrum, such as the boson peak, the quasi-elastic scattering and the vibrational localization or propagation are being investigated. In fact, the physical nature of the modes responsible for the boson peak is still unclear and represents a problem of current interest. In the last years the boson peak properties have been studied as a function of temperature, near and far from the glass transition, and as a function of pressure in strong and fragile glasses, in porous systems, by means of several experiments as Raman and neutron scattering measurements.

Inelastic light scattering experiments in the low frequency domain (Boson peak) are interpreted as being due to inhomogeneities in the structure of the glass but these models are still a matter of discussion. Besides, elastic scattering (Rayleigh scattering) in elemental and a simple component glass is well interpreted as due to density fluctuations. The role of thermal treatment on the energy of the Boson peak was demonstrated in Refs. [83–85,95].

In this Paragraph, we will make an attempt to separate the different contributions of Rayleigh, Brillouin, and Raman processes. We propose further to follow their evolution with the fictive temperature to correlate these observations with the structure of the glass.

7.1. Theoretical models for boson peak

There are essentially three different scenarios that have been proposed for the origin of the boson peak in glasses [88–102] One assumes that vibrational modes additional to sound waves exist, another ascribes the boson peak to localized vibrational modes, perhaps associated with inhomogeneities in the glass structure, while the third ascribes the non-Debye excess of modes to the effect of disorder (strong scattering) on sound wave excitation. None of these theories has yet fully described every aspect of the physical origin of the BP.

7.1.1. First model: soft potential model

In the first model, the localized modes in the very low frequency (< 1 GHz), which is called tunneling modes, are postulated to extends to the Boson peak region and gives rise to the Boson peak. This model is called soft potential model, in which both the relaxational and vibrational modes are explained in same physics. The Boson peak is attributed to the existence of anharmonic localized potential wells (and double wells). Simulations have been performed successfully for vitreous silica, suggesting the Boson peak of which arises from coupled rotations and bodily translations of SiO_4 tetrahedrons.

The tunneling model postulates the existence in glasses of localized modes, whose character is still disputed, that are responsible for low-temperature anomalies in thermal properties. Such modes are believed to exist at frequencies below 1 GHz.

In the so-called soft potential model, it is postulated that such localized modes persist up to much higher frequencies, crossing over to vibrational modes in soft harmonic potential wells at frequencies in the boson peak region. This approach, naturally accounts for both relaxational and vibrational modes. Quasi-localized modes have been identified in simulations of vitreous SiO_2. Such modes comprise coupled rotations and bodily translations of SiO_4tetrahedra.

7.1.2. Second model: localized vibration model

This model assumes that the structure of glasses is inhomogeneous, consisting of an aggregated blobs with different density from the matrix. The boson peak is assumed to be due to vibrational modes spatially localized in such blobs. However, there is no evidence, from computer simulation, that the sort of density fluctuations envisaged exist in the structure of glass network. There is no evidence that true localization of modes exists at low frequencies of the order of 1 THz. Also, Vibrational localization should occur only at the edges of the acoustic and optic bands in the VDOS at much higher frequencies.

The second model ascribes the Boson peak to localized vibrational modes. It assumes that the structure of the glasses is inhomogeneous, consisting of an aggregate of “blobs” with a different density or elastic constants from the matrix. The Boson peak is assumed to be due to vibrational modes spatially localized in such blobs. No computer simulations, however, have proved such density fluctuations neither exist, nor are there any evidence that localized mode can occur at such low frequency.

7.1.3. Third model: medium range disorder model

The third model attributes the extra, non-Debye-like modes in the boson peak region to the result of strong scattering of sound waves by the disorder (in force constants or atomic positions) characteristic of the amorphous states. W. Schirmacher et al [23] presented compelling evidence that a strongly disordered three-dimensional system of coupled harmonic oscillators with a continuous force constant distribution exhibits an excess low-frequency DOS (Boson Peak) as a generic feature. This was achieved by comparing the results of a CPA (coherent-potential approximation) calculation with those of a numerical diagonalization [55]. The extra states in the boson peak region are supposed to be the high k acoustic or low k optics modes pushed down in frequency by disorder and mixed with the low k acoustic modes.

The medium range disorder will induce the broadening of the vibration lines in the high frequency range, some vibration states will extend to the low frequency range, which gives rise to the excess of density of states in the low frequency range as compared with what is predicted by the Debye's model.

When the disorder increases, more broadening will cause the vibrational peaks in the high frequency region to broaden more, thus more excess of density of states will extend to the low frequency region, giving rise to a higher Boson peak intensity; while on the other side, more broadening will cause the peaks extend to lower frequency, which means the Boson peak energy will decrease [4–6,9–12]. According to the theoretical prediction of this model, Boson peak energy decreases and its intensity increases with increasing disorder.

To obtain a better understanding of the density of states in the Boson peak regime more spectral information is needed. This is hard to get merely from Raman spectroscopy because of the coupling coefficient is frequency dependent. In the case of inelastic neutron scattering, the VDOS is obtained more directly, with no strongly frequency-dependent coupling coefficient being involved. In the third model, it was proposed the Boson peak originates from the medium range disorder of the system.

The previous two models are actually the utilization of the model that was used to describe the higher and lower frequency regions. We will base our analysis on the third model, which in its simple yet convincing way gives a clear explanation for the Boson peak.

In a simplified language, this model basically states that the disorder leads to a local repulsion of vibrational states, which includes a downward shift of low frequency states as compared to the Debye prediction.

In this model, it is proposed that the more disordered the system is, the higher the Boson peak is.

Chalcogenide glasses are often called covalent network glasses which can be categorized between fragile (e.g., polymer and molecular glasses) and strong (e.g., silica and other oxides) glasses, and therefore significantly different from silica and polymer/molecular glasses in structural/glassy properties and hence in the origin of the Boson peak. The Boson peak of typical chalcogenide glasses, is observed as an excess peak at about 3 meV in the vibrational density of states. Several models [1–4] have been proposed to explain the origin of the Boson peak in chalcogenide glasses. Features and the origin of Boson peak were often

discussed in relation to microscopic and/or intermediate range structure, and sometimes explained together with the origin of the first sharp diffraction peak (FSDP) which is characteristic for the glasses. However, the proposed ideas seem to be still controversial. Besides localized or propagating vibrational modes, the low-energy excitations of glasses can be involved also with relaxation and/or deformational motions of restricted structures. This fact has made the exploration of the low-energy modes (including the Boson peak) of glasses difficult and complicated.

Experimental results indicate that the BP intensity decreases when a glass is compressed or when the fictive temperature decreases with the important exception of hyper quenched vitreous silica from very high temperatures. This exception, however, can be explained if the anomaly of the density of silica at high temperature is taken into account.

When considered from the viewpoint of vibrational dynamics, crystalline and non-crystalline (glasses and amorphous solids) materials exhibit noticeable differences at energies that are material dependent, but that always lie around 1 THz. These differences, that have their origin at the lack of long–range periodicity, can all be traced back to the universal presence in glasses of low–energy excitations in excess of the parent crystals. The term low–energy excitations has been coined to account for properties concerning: (i) the specific heat excess (bump in the plot) at temperatures around 5–10 K, (ii) the plateau in thermal conductivity at about the same temperature, (iii) the strong attenuation of sound waves, and (iv) the presence of scattering intensity– absent from the parent crystal – in Raman and inelastic incoherent neutron scattering (INS) spectra.

The last issue, low energy scattering intensity excess, has recently resurfaced in view of new theoretical and experimental approaches [4–15]. In particular, crystalline solids obey rather accurately the predictions of the Debye model for an elastic continuum, according to which the vibrational density of states is a quadratic function of the frequency. On the contrary, non-crystalline phases ubiquitously exhibit some extra low-energy vibrational modes in excess.

The inherent difficulty in the formulation of successful theories for glasses has led to the suggestion of numerous empirical correlations among different glass properties. Such correlations usually relate a spectral characteristic of the Boson peak (intensity, peak position etc.) with a specific property of the glass.

An efficient way to obtain information on Boson peak is to study its spectral changes by changing the glass composition and/or the magnitude of certain external parameters.

Rayleigh scattering is 5–10 orders higher in intensity comparing with the Raman scattering. The Rayleigh scattering can thus obscure most of the Raman scattering signals and must be rejected using appropriate method.

In these Tellurium oxide glasses, the very high Boson peak indicates high disorder. Since the Boson peak is caused by the broadening of the high frequency vibrational peaks, the high Boson peak in the low frequency range comes as no surprise because these Tellurium oxide glasses do have high Raman scattering intensity in the high frequency region. Especially, the very high vibrational peak in the low frequency region, just above the Boson peak region, e.g. $> 100\ cm^{-1}$, might has been a major contribution.

A systematic analytical study of the relationship between Boson peak and the composition or structure, however, requires a glass family with gradual systematic structural change. A binary glass family with one component percentage increases gradually and the other component decreases gradually would be a good glass system for this study. This leads to the making of the binary phosphate glasses and the study of relationship between Boson peak and medium range disorder.

7.2. Depolarization ratio curves in the boson peak region

For the same material, the Boson peak shape of polarized and depolarized Raman spectra are almost the same. As a result, the depolarization ratio, the ratio of intensities of depolarized Raman spectra over polarized Raman spectra, should be a constant. The depolarization ratio is supposed to be at its minimum when the vibrations are symmetric, because when the vibration is symmetric, the scattering tends to be symmetric and the possibility for the incoming light to change polarization is very small. So the depolarization curves further confirmed the accuracy of the assignments of the two peaks.

It was found that the vh and vv spectra have the same reduced Raman intensity profile in the Boson peak region (30-100 cm^{-1}) which tells us that the depolarization ratio should be a constant in the Boson peak region.

8. Conclusions

As stated in this Chapter, from Raman spectra alone, it is not possible to obtain directly the density of states, because the expression of the Raman intensity, IR, contains a frequency dependent unknown function.

Raman spectroscopy basically reveals the density of states information, but not all density of states are Raman active, only a certain portion of all the density of states are coupled into Raman scattering. There is a factor to quantify this coupling which is called the coupling coefficient.

Some evidence is provided that the boson peak and floppy modes share a common origin. In the particular case of periodic systems, we show how a boson peak occurs as a consequence of a reduction of constraints in an over-constrained lattice, in contrast to floppy modes, which occur for a reduction of constraints in a flexible or isostatic lattice. In fact, the present approach allows us to follow the transformation of the boson peak into a floppy mode when a system goes from rigid to flexible. For over-constrained lattices, it was found that the boson peak frequency depends on the square root of the coordination of the lattice, and is at most 0.3 of the Debye frequency, a value close to the observed experimental ratio of 0.1.

From the above we can conclude the following.

The molecular structure of amorphous selenium differs from that of the majority of inorganic glasses on a scale of medium-range order. Apparently, Se chains form a structure similar to the structure of linear polymers on the scale ~ 1 nm.

Depending on the irradiation energy density, two qualitatively different regions are observed. Below the energy density threshold, E_{th}, only small changes in the local structure of the system can be detected. Above E_{th}, the changes were attributed to crystallization transformation. In addition, we have detected the successive phases in such a transition which is a threshold phenomenon.

It has been shown that Raman scattering spectra of amorphous As_xSe_{1-x} alloys change non-monotonically with composition in the region of bond stretching modes. Certain extrema in various physical properties exist at composition range 6–12 at % As. The presence of this topological threshold is established by direct evidence, such as peculiarities in the compositional dependence of the Raman vibration modes of glasses. These peculiarities are caused by the transition from a chain-ring-like structure to chain-like structure with increasing degree of cross-linking.

Based on Raman scattering studies, we have shown how the structure transforms chronologically in amorphous As_xSe_{1-x} recording media. Laser-induced changes at room temperature involve two phenomena essentially different in their origin: transient reversible changes (photo darkening) and irreversible changes (photo crystallization) with gross structural reorganization. For high values of energy density, the Raman spectrum has pronounced crystallization-related changes.

Our explanation are based on the assumption that the radiation pumps the material from an amorphous state towards the crystalline state through the formation of small clusters, which coalesce to form large clusters attaining micro-crystallite size at high energy density levels.

In our opinion, the very low-frequency region of the Raman scattering could be an important source of information on the structure of disordered solids on the scale ~10–100 Å. It should be stressed on that the above method is efficient in distinguishing of micro-inhomogeneities.

References

[1] Kasap SO, Frey JB, Belev G, Tousignant O, Mani H, Laperriere L, et al. Phys Status Solidi B 2009;246:1794.
[2] Popescu M. J Non-Cryst Solids 2006;352:887.
[3] Madan A, Shaw MP. The physics and applications of amorphous semiconductors. Boston, MA: Academic Press; 1988.
[4] Feltz A. Amorphous inorganic materials and glasses. Weinheim, Germany: VCH; 1993.
[5] Mikla VI, Mikla VV. J Mater Sci Mater Electron 2009;20:1095.
[6] Mikla VI, Mikla VV. J Optoelectron Adv Mater 2008;10(1):131.
[7] Mikla VI, Mikla VV. J Optoelectron Adv Mater – Rapid Comm 2007;1(6):272.
[8] Kasap SO. Diamond AS, Weiss DS, editors. Handbook of imaging materials. 2nd ed.New York: Marcel Dekker, Inc.; 2002. p. 329. and references therein.
[9] Tanaka K. Encyclopedia of materials. North Holland: Elsevier Science Ltd; 2001. p. 1123.
[10] Shimakawa K. Adv Phys 1995;44:474.
[11] Kasap SO, Rowlands JA. J Mater Sci Mater Electron 2000;11:179.
[12] Borisova Z. Glassy semiconductors. New York: Plenum Press; 1981.
[13] Mott NF, Davis EA. Electronic processes in: Non-Crystalline materials. 2nd ed. Oxford: Oxford University Press; 1979.
[14] Hulls K, Mc Millan PW. J Non-Cryst Solids 1974;15:357.
[15] Schottmiller J, Tabak M, Lucovsky G, Ward A. J Non-Cryst Solids 1970;4:80.
[16] Owen AE, Firth AP, Ewen PJS. Philos Mag B 1985;52:347.
[17] Owen AE, Spear WE. Phys Chem Glas 1976;17:174.
[18] Mikla VI, Semak DG, Mateleshko AV, Levkulich AR. Sov Phys Semicond 1987;21:266.
[19] Mikla VI, Semak DG, Mateleshko AV, Levkulich AR. Sov Phys Semicond 1989;23:80.
[20] Mikla VI. J Phys Condens Matter 1997;9(9209).
[21] Tanaka K. Rev Solid State Sci 1990;2–3:644.
[22] Dresner J, Strinfellow GB. J Phys Chem Solids 1968;29:303.
[23] De Neufville JP. Seraphin DO, editor. Optical properties of solids – new developments. Amsterdam: North-Holand; 1975. p. 437.
[24] Fritzsche H. Boolchand P, editor. Insulating and semiconducting glasses, vol. 10. Singapore, Ch: World Scientific; 2000.
[25] Mikla VI, Mikhalko IP. J Non-Cryst Solids 1995;180:236.
[26] Chomat M, Lezal D, Gregore J, Srb I. J Non-Cryst Solids 1976;20:427.
[27] Mikla VI. J Phys Condens Matter 1997;9(9209).
[28] Zakharov VP, Gerasimenko VS. Structural peculiarities of semiconductors in amorphous state. Kiev: NaukovaDumka; 1984.
[29] Galeneer FL. J Non-Cryst Solids 1990;123(182).
[30] Cardona M. Light scattering in solids. Berlin: Springer-Verlag; 1975.
[31] Nemanich RJ, Connell GA, Hayes TM, Street RA. Phys Rev B 1978;18:6900.
[32] Luksha OV, Mikla VI, Ivanitsky VP, Mateleshko AV, Semak DG. J Non-Cryst Solids 1992;144:253.
[33] Cervinka L. Czech J Phys B 1985;25:1193.
[34] Elliott SR. J Non-Cryst Solids 1988;106(26).
[35] Lannin JS. Phys Today 1988;41(28).
[36] A. J. Leadbetter, A. J. Apling, 21, 47 (1976).
[37] Wright AC, Sinclair RN, Leadbetter AJ. J Non-Cryst Solids 1985;71:295.
[38] Daniel MF, Leadbetter AJ, Wright AC, Sinclair RN. J Non-Cryst Solids 1979;23:271.
[39] Baganich AA, Mikla VI, Semak DG, Sokolov AP. Phys Stat Sol (b) 1991;166:297.
[40] Gorman M, Solin SA. Solid State Commun 1976;18:1401.
[41] Brodsky MH, Cardona M. J Non-Cryst Solids 1978;31:81.
[42] Carroll PJ, Lannin JS. Solid State Commun 1981;40:81.
[43] Carroll PJ, Lannin JS. J Non-Cryst Solids 1980;35–36:1277.
[44] Mori T, Onari S, Arai T. J Appl Phys 1980;19:1027.
[45] Onari S, Matsuishi K, Arai T. J Non-Cryst Solids 1985;74:57.
[46] Phillips JC. J Non-Cryst Solids 1981;43:37.
[47] Thorpe MF. J Non-Cryst Solids 1983;57:355.
[48] Tanaka K. Phys Rev B 1989;39:1270.
[49] Wagner T, Kasap SO. Philos Mag B 1996;74:667.
[50] Borisova Z. Glassy semiconductors. New York: Plenum Press; 1981.
[51] Boolchand P, Jin M, Novita DI, Chakravarty S. J Raman Spectrosc 2007;38:660.
[52] Ahn E, Williams GA, Taylor PC. Phys Rev B 2006;74:174206.
[53] Tanaka K, Odajima N. Solid State Commun 1982;43(961).
[54] Phillips RT. J Non-Cryst Solids 1985;70(359).
[55] Powder Diffraction File. Berry LG, editor. ASTM card. Philadelphia: Joint Committee on Powder Diffraction Standard; 1974.
[56] Zallen R, Slade ML, Ward AT. Phys Rev 1971;B3:4257.
[57] Abkowitz M, Enck RC. Phys Rev 1983;B27:7402.
[58] Mikla VI. Institute of solid state physics Dr Sci. Thesis Kiev: Academy of Sciences; 1998.
[59] Phillips JC. Solid State Phys 1982;10:165.
[60] Mikla VI, Semak DG, Mateleshko AV, Baganich AA. Phys Stat Solidi (a) 1990;117:241.
[61] Malinovsky VK, Sokolov VP. Solid State Commun 1986;57:757.
[62] Martin AJ, Brenig W. Phys Status Solidi B 1974;63:163.
[63] Nemanich RJ. Phys Rev B 1977;16.
[64] Kawamura H, Fukumasu F, Hamada Y. Solid State Commun 1982;43:229.
[65] Lucovsky G, Galeneer FL. J Non-Cryst Solids 1980;35–36:1209.
[66] Jakle J. Phillips WA, editor. Amorphous solids: low-temperature properties. Berlin: Springer-Verlag; 1981. p. 135.
[67] Malinovsky VK, Novikov VN, Sokolov VP. Phys I Khim Stekla 1989;15:331.
[68] Lucovsky G. J Non-Cryst Solids 1987;97–98:155.
[69] Richter H, Wang ZP, Ley L. Solid State Commun 1981;39:625.
[70] Bagrynskii VA, Malinovsky VK, Novikov VN, Puschaeva LM, Sokolov AP. Fiz Tverd Tela 1988;30:2360.
[71] Shuker R, Gammon R. Phys Rev Lett 1975;25:222.
[72] Martin AJ, Brenig W. Phys Status Solidi (b) 1974;64:163.
[73] Duval E, Boukenter A, Champagnon B. Phys Rev Lett 1986;56:56.
[74] Lamb H. Proc Lond Mat Soc 1982;13:187.
[75] Tamura A, Higeta K, Ichinokawa T. J Phys C 1982;15:4957.
[76] Tamura A, Ichinokawa T. J Phys C 1983;16:4779.
[77] Malinovsky VK, Novikov VN, Sokolov AP. Solid State Commun 1988;67:725.
[78] Jackle J. Amorphous solids: low-temperature properties. New York: Springer; 1981.
[79] Lipinska-Kalita KE, Mariotto G. J Non-Cryst Solids 1991;128:285.
[80] Nemanich RJ. Phys Rev B 1977;16:1655.
[81] Kawamura H, Fukumasu K, Hamada Y. Solid State Commun 1982;43:229.
[82] Boukenter A, Duval E, Achibat T. J Condens Matter 1990;2:10227.
[83] Malinovsky VK, Sokolov AP. Solid State Commun 1986;57:757.
[84] Malinovsky VK, Novikov VN, Parshin PP, Sokolov AP, Zemlyanov MG. Europhys Lett 1990;11.
[85] Boukenter A, Champagnon B, Duval E, Rousset JL, Rosenberg HM. Philos Mag B – Phys Condens Matter Stat Mech Electron Opt Magn Prop 1989;59:125.
[86] Shuker R, Gammon R. Phys Rev Lett 1970;25:222.
[87] Martin AJ, Brenig W. Phys Status Solidi B 1974;64:163.
[88] Sokolov AP, Buchenau U, Steffen W. Phys Rev B 1995;52:R9815.
[89] Sokolov AP, Kisliuk A, Quttmann D, Duval E. Phys Rev B 1993;48:7692.
[90] Hong I, Begen B, Kisliuk A, Simioneco C, Novikov V, Sokolov AP. Phys Rev B 2008;78:134201.
[91] Hong I, Begen B, Kisliuk A, Novikov V, Sokolov AP. Phys Rev B 2010;81:104207.
[92] Hong I, Begen B, Kisliuk A, Pawlus S, Paluch M, Sokolov AP. Phys Rev Lett 2009;102:145502.
[93] Krishnan RS. Proc Indian Acad Sci A 1953;37:3778.
[94] Yannapoulos N, Andrikopoulos KS. J Chem Phys 2004;121:4747.
[95] Andrikopoulos KS, Kristofilos D, Yonnapoulos SN. J Non-Cryst Solids 2006;352:4594.
[96] Zorn Reiner. Physics 2011;4:44.
[97] Chumaov AI, et al. Phys Rev Lett 2011;106:225501.
[98] Mikla VI. J Phys Condens Matter 1996;8:429.
[99] Mikla VI, Mikla VV. J Mater Sci Mater Electron 2009;20:1095.
[100] Baganich AA, Mikla VI, Semak DG, Sokolov AP. Phys Status Solidi (b) 1991;166:297.
[101] Mikla VI, Baganich AA, Sokolov AP, Shebanin AP. Phys Status Solidi (b) 1993;175:1029.
[102] Schirmacher W. J Phys Condens Matter 2013;25:495.